Brodogradnja Volume 77 Number 1 (2026) 77102

journal homepage: www.brodogradnja.fsb.hr

Brodogradnja

An International Journal of Naval Architecture and Ocean Engineering for Research and Development

Hydrodynamic interactions in midwater trawl nets: combined effects of flow velocity and door spreading through numerical and experimental approaches

Zhao Cheng[1], *Xiaobin Li*[1], *Yonghe Xie*[2], *Panpan Jia*[1], *Li Guoqiang*[1,2], *Wang Wei*[2*]

[1] *School of Naval Architecture, Ocean and Energy Power Engineering, Wuhan University of Technology, Wuhan 430063*
[2] *School of Naval Architecture and Maritime, Zhejiang Ocean University, Zhoushan 316022*

ARTICLE INFO

Keywords:
Midwater trawl
Lumped mass method
Towing experiment
Sea trial

ABSTRACT

Owing to escalating fuel costs and dwindling fish stocks, optimising midwater trawl efficiency requires a thorough investigation of net design variables. To understand the morphological changes in a trawl net under different operating conditions, a numerical model of the trawl was established using the lumped-mass method. The effects of door spread and flow velocity on trawl morphology, drag force, and energy consumption coefficients were analysed. A generalised additive model was employed to predict the net configuration. In addition, the net mouth parameters of the trawl net were measured using scale model tests in a towing tank and full-scale sea trials to verify the reliability of the predicted results. This study provides guidelines for improving the geometric performance and catchability of midwater trawls.

1. Introduction

Trawling is an important tool for exploiting fishery resources in pelagic waters and is a key method for harvesting fishery resources, accounting for approximately 25 % of the global catch [1]. With the implementation of policies restricting or prohibiting bottom trawling [2], enhancing midwater trawling techniques and improving trawl efficiency have become increasingly crucial.

Midwater trawling exhibits exceptional adaptability and flexibility compared with other fishing methods. During fishing operations, it is necessary to adjust the trawl water layer according to the biological characteristics and activity depth of the target fish to achieve precise fishing. In studies on trawl performance, scholars typically select key performance observation indicators such as the wing-end spread, net mouth vertical opening, drag force, and energy consumption coefficient.

Research on trawl performance has primarily been conducted using three methodologies: numerical simulations [3, 4], tank testing [5-8], and sea trials [9, 10]. Numerical simulations excel in cost-effectiveness and rapid iteration capabilities, enabling precise control of hydrodynamic parameters. Priour [11] used the triangular finite element method to calculate net shapes, where the number of nodes was smaller and the computational efficiency was improved. Zhao et al. [12] conducted numerical simulations on a net model of porous media using the finite-volume method to calculate the hydrodynamic performance of the net at

* Corresponding author.
E-mail address: wangwei1981@zjou.edu.cn

https://doi.org/10.21278/brod77102
Received 27 March 2025; Received in revised form 20 July 2025; Accepted 19 August 2025
Available online 2 September 2025
ISSN 0007-215X; eISSN 1845-5859

different angles of attack. Ye et al. [13] proposed a simplified mass-spring model and employed a collision-detection algorithm to establish a dynamic model of the net, simulating its dynamic deformation. Considering the damping forces in mesh bars, Yao et al. [4] developed an optimised physical parameter method to improve computational efficiency by performing numerical simulations of the trawl system using the lumped mass approach. Thierry et al. [14] employed a two-way coupling fluid-structure interaction approach to simulate a simplified bottom trawl model using ANSYS, calculated the hydrodynamic performance of the trawl under different flow velocities, and analysed the surrounding flow field distribution.

Tank testing validated the net performance in highly controlled environments. Thierry et al. [7]. conducted flume tests on four bottom trawl nets made of different materials and proposed that the resistance of the bottom trawl made of new materials was much lower than that of traditional materials. Thierry et al. [8] conducted model tests on Antarctic krill midwater trawls in a flume tank and investigated the effects of varying flow velocities and horizontal spread ratios on the hydrodynamic performance of the model net. They also evaluated the engineering performance of trawls under different gear configurations. Based on the results of flow field measurements around trawl nets using an electromagnetic current velocity meter (ECVM) in a flume tank, Tang et al. [6] characterised the hydrodynamic interactions between midwater trawls and ambient flows through combined wavelet and Fourier transform analyses, specifically by examining the influence of different trawl door spread and flow speeds.

Sea trials capture dynamic trawl behaviours under complex operational conditions in marine environments. Kim et al. [15, 16] conducted in situ measurements of three-dimensional flow velocities within the cod end of a bottom trawl during fishing operations using a 3-D velocimeter mounted to analyse the turbulent flow characteristics inside the net under normal towing conditions. To improve fishing gear and reduce energy consumption, Priour and Prada [17] conducted comprehensive measurements of the geometric characteristics of bottom trawls using multiple sensors. Wan et al. [18] used depth sensors to measure net positions in sea trials and analysed the hydrodynamic performance of a trawl system across different warp lengths and towing speeds through integrated field and numerical studies. Jia et al. [10] developed a machine learning model to correlate trawl net geometry with towing parameters (speed and warp length) from sea trial data, providing a predictive capability for net performance in uncharacterized sea states.

However, the results of the single-method approaches have limitations. Contemporary research indicates the absence of reliable predictive methods for accurately assessing fishing gear performance [5]. Considering trawl port parameters as the object, this study analysed the shortcomings of the three research methods. Compared with sea trials and towing tests, numerical simulations can effectively control the door spread and flow velocity to accumulate samples. Based on numerical simulation results with a large number of samples, the use of machine learning methods can further improve the computational efficiency.

To comprehensively evaluate the dynamic performance of midwater trawl systems, this study implemented a multi-methodological approach combining numerical simulations using the lumped-mass method, controlled towing tank experiments with scaled net models, and full-scale sea trials. This investigation focused on critical performance parameters including door spread configurations, flow velocity effects, vertical opening of the net mouth, wing-end spread dimensions, net mouth area, drag force characteristics, and energy consumption coefficients. Generalised additive modelling (GAM) was employed to predict the trawl net under uncharacterized conditions, and model validation was achieved through a correlation analysis between numerical results, towing tank measurements, and sea trial data. These integrated findings provide valuable insights for optimising midwater trawl design and operational efficiency.

2. Materials and methods

2.1 Geometrical shape of the trawl net

This study examined the trawl net configuration employed in fishing operations in the East China Sea region. The net was made of high-strength polyethene with a density of 950 kg/m^3, an elastic modulus of 1.1x10^9 Pa, and a diamond mesh with a 95 % hanging ratio. The trawl net opening was expanded by the combined action of 19 floats with a buoyancy of 10 kg and a sinker of 125 kg. The bridle length was 30 m

including the net pennant and hand rope, the diameter was 0.016 m, the linear density was 0.85 kg/m, and the elastic modulus was $2x10^{11}$ Pa. The trawl consists of a large number meshes, with its construction incorporated varied twine specifications, including multiple mesh dimensions and diameter parameters. Complete technical details provided in Figure 1.

In studies on trawl performance, scholars typically select key performance observation indicators, such as drag force, mouth area, and energy consumption coefficient. This study aimed to systematically assess the influence of varying door spread configurations (D) and flow velocities on both the hydrodynamic characteristics and three-dimensional deformation patterns of a trawl net mouth.

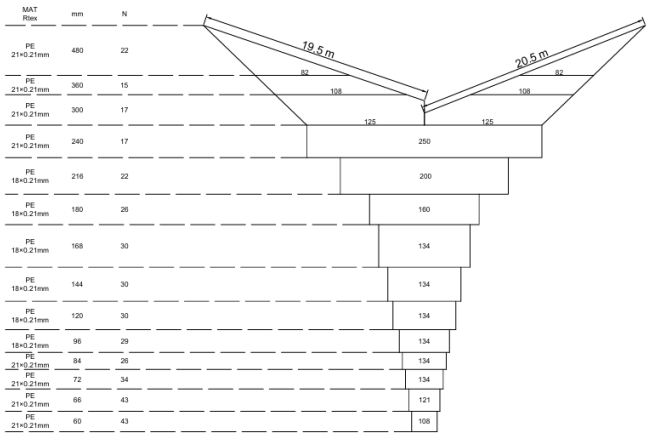

Fig. 1 The drawing of full-scale net

Data on the drag force of the trawl net, energy consumption coefficients, and trawl geometry (including the net mouth, mouth area, and wings) were obtained from a midwater trawl. The shapes of the net mouth and the drag force are shown in Figure 2 [19].

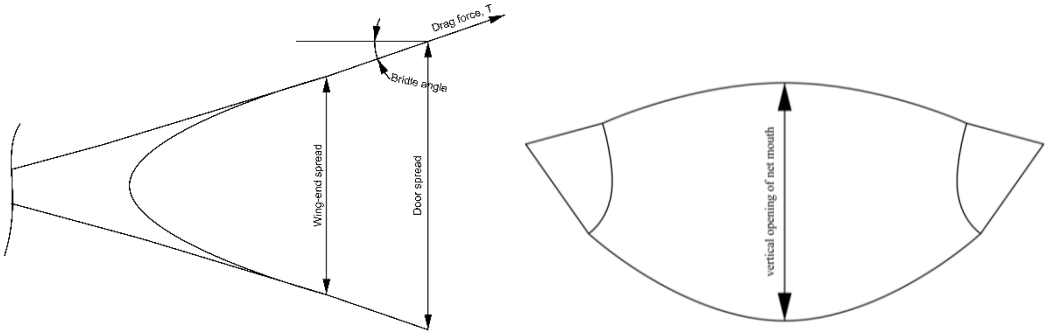

(a) Top view (b) Principal view

Fig. 2 Net mouth parameters

The midwater mouth area (S) [8] was calculated:

$$S = 0.8H \times W_s \tag{1}$$

where H is the vertical opening of the net mouth and W_s is the wing-end spread.

Energy efficiency assessment in trawl operations is a critical metric for quantifying trawl net performance characteristics. In this study, the energy consumption coefficient (C_e) was used to represent the energy efficiency [8]:

$$C_e = \frac{3.472 \times F_{Td}}{H \times W_s} \tag{2}$$

$$F_{Td} = F_d + \frac{F_{in-p}}{\alpha} \tag{3}$$

where F_{Td} is the total drag force of the trawl net system, F_d is the trawl drag, $F_d = 2T\cos(\theta)$, F_{in-p} is the in-pull force of trawl, $F_{in-p} = T\ \sin(\theta)$, θ is the bridle angle, $\sin(\theta) = \frac{D-W_s}{bridle\ length}$, α is the lift-to-drag ration of the otter board which varies from 1.5 to 3.5 [20], in the present study, $\alpha = 3$.

2.2 Numerical simulation

A lumped mass model was implemented to simulate full-scale trawl net dynamics. In the modelling process, the knots were regarded as regular spheres, the bars were regarded as massless spring units, and the hydrodynamic, buoyancy, and gravitational forces acting on the bars were equally distributed to the adjacent knots, whereas the sinkers and float forces were uniformly distributed over the node mass points. The net model was simplified by a 4×4 scale mesh grouping method and was used to reduce the computational size.

2.2.1 Equation of the nodes

The modelling approach treats each knot and half-length segment of the adjoining bars as an integrated node, and the equation of motion for the nodes can be expressed as follows:

$$(m + \Delta m)\boldsymbol{a} = \sum \boldsymbol{T} + \boldsymbol{H} + \boldsymbol{G} + \boldsymbol{B} \tag{4}$$

where $\boldsymbol{T}$ is the tension force of the bars and $\boldsymbol{H}, \boldsymbol{G}, \boldsymbol{B}$ are the hydrodynamic force, gravity, and buoyancy of the node, respectively. $\boldsymbol{a}$ is the acceleration vector of the knot, m and Δm represent the actual mass and the added mass, respectively. Here:

$$\Delta m = C_m \rho V \tag{5}$$

where C_m is the added mass coefficient, ρ is the fluid density, V is the mass-point volume.

The bars are considered as linear elastic bodies, and according to Hooke's law, the tension force can be expressed as follows:

$$\boldsymbol{T} = EA_b \cdot \frac{l - l_0}{l_0} \cdot \mathrm{norm}(\boldsymbol{l}) \tag{6}$$

where E is Young's modulus, A_b is the cross area of the bar, l and l_0 are the length and initial length of the bar, respectively, $\mathrm{norm}(\boldsymbol{l})$ is the unit vector of the bar.

The hydrodynamic force at the mass point includes the hydrodynamic forces acting on the knot and half of the adjacent bars.

The hydrodynamic force $\boldsymbol{H_k}$ of the knot can be described as follows:

$$\boldsymbol{H_k} = -\frac{1}{2} C_d \rho A_k |\boldsymbol{v_k} - \boldsymbol{J}|(\boldsymbol{v_k} - \boldsymbol{J}) \tag{7}$$

where C_d is the drag coefficient of the knot, $C_d = 1.0$ [21], A_k is the projected area of the knot, $\boldsymbol{v_k}$ is the velocity vector of the knot, $\boldsymbol{J}$ is the flow velocity vector.

The bar is considered a regular cylindrical body [22], and the hydrodynamic force $\boldsymbol{H_b}$ of the bar consists of drag force $\boldsymbol{F_p}$ and viscous friction force $\boldsymbol{F_f}$ [4]. The velocity vector of the bar $\boldsymbol{v_b}$ is the average velocity of two adjacent knots $\boldsymbol{v_{ka}}$, $\boldsymbol{v_{kb}}$. The resultant velocity $\boldsymbol{v_m}$ of the bar can be expressed as:

$$\boldsymbol{v_m} = \frac{(\boldsymbol{v_{ka}} + \boldsymbol{v_{kb}})}{2} - \boldsymbol{J} \tag{8}$$

The form drag force $\boldsymbol{F_p}$ and viscous friction force $\boldsymbol{F_f}$ are proportional to the projection of $\boldsymbol{v_b}$ in their respective directions:

$$\boldsymbol{F_p} = C_{N90}\frac{\rho(\boldsymbol{v_m}\cdot\sin\alpha)^2}{2}\cdot S_N\cdot\boldsymbol{n_p} \tag{9}$$

$$\boldsymbol{F_f} = C_f\frac{\rho(\boldsymbol{v_m}\cdot\cos\alpha)^2}{2}\cdot S_f\cdot\boldsymbol{n_f} \tag{10}$$

where C_{N90} is the drag coefficient of the bar when it is perpendicular to the flow, C_f is the viscous friction coefficient, $C_{N90} = 1.12$ and $\pi C_f = 0.02$ [23], α is the angle of attack of the bar, S_N and S_f are the projected area and the wetted surface area of the bar, respectively, where $S_N = dl$ and $S_f = \pi dl$, with d and l being the diameter and length of the bar, respectively, the vectors $\boldsymbol{n_p}$ and $\boldsymbol{n_f}$ are the direction vectors of the $\boldsymbol{F_p}$ and $\boldsymbol{F_f}$, respectively:

$$\boldsymbol{n_p} = \frac{(\boldsymbol{v_m}\times\boldsymbol{l})\times\boldsymbol{l}}{|(\boldsymbol{v_m}\times\boldsymbol{l})\times\boldsymbol{l}|} \tag{11}$$

$$\boldsymbol{n_f} = -\boldsymbol{l}\cdot\mathrm{sign}(\boldsymbol{v_m}\cdot\boldsymbol{l}) \tag{12}$$

2.2.2 Solution method

Based on the equations for the knots shown above, the motion of the node constituting the trawl net was determined based on its velocity, displacement, and acceleration. The equations of motion for all the nodes can be expressed as:

$$\ddot{\boldsymbol{q}} = f(\boldsymbol{q},\dot{\boldsymbol{q}}) \tag{13}$$

where $\boldsymbol{q} = [x_1, y_1, z_1, \ldots, x_n, y_n, z_n]^T$, x, y, and z are the coordinates of the nodes, n is the number of nodes, $n = 2948$.

Based on the mesh size and assuming that the cross-sections of the net body are circular, the initial conditions of the numerical model of the net were specified, including the position and velocity information of all nodes. Using the information of the nodes, the hydrodynamic force on the nodes and the tension of the bars can be calculated. The equations of motion can be obtained by concentrating the forces obtained above on the nodes. By numerically integrating the equations of motion of the nodes, it is possible to calculate the positions of all nodes at the next moment. In this study, the fourth-order Runge-Kutta method is employed to solve Equation (15). The total simulation duration was 50 s with a time step of 0.1 ms. The simulation software was developed using MATLAB. Considering the symmetry of the trawl net, simulations were performed on only half of the net to improve computational efficiency.

Net shapes and drag forces were calculated under various conditions by setting different door spreads and flow velocities. The simulation results of the net model when the door spread is 30 m and the flow velocity is 4 kN are shown in Figure 3.

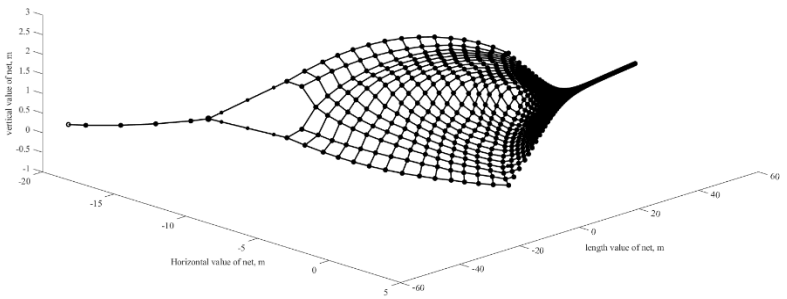

Fig. 3 The simulation result of the net model

Considering the towing speed (2-5 kn) and otter board expansion (30-50 m) during the sea trials, the simulation conditions are listed in Table 1.

Table 1 Simulation conditions

Flow velocity, *J* (kn)	Door spread, *D* (m)
2, 3, 3.5, 4, 4.5, 5	20, 30, 35, 40, 45, 50

2.3 Towing tank test

Based on the trawl model towing tank test method [24], model experiments were conducted under different door spreads and towing speeds. Based on the full-scale net, a model net was created using the modified Tauti's law [25]. The experiment was conducted in the towing tank of Zhejiang Ocean University, which measured 130 × 6 × 3.5 m. Two vertical poles were installed on the towing carriage, with the ends of the poles connected to a warp. Tension sensors were used to measure the drag force of the trawl model. During the test, the door spread of the trawl model was controlled using two vertical poles.

Considering factors such as the spacing between otter boards, towing speed in actual fishing operations and size of the towing tank, the large-scale ratio of the model net (λ) was determined to be 13, and the small-scale ratio (λ') was 3. Figure 4 illustrates the test setup. The towing speed and door spread conditions are listed in Table 2.

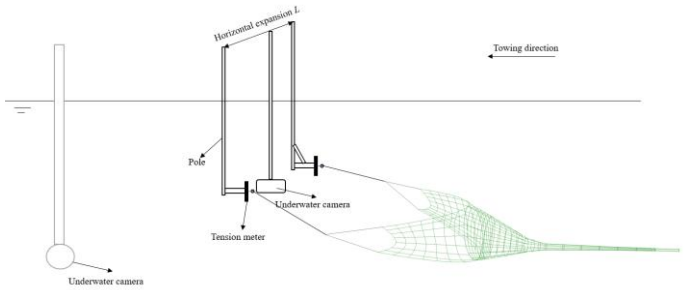

Fig. 4 Test process of a scale model of the trawl test in the towing tank

Table 2 Towing tank test conditions

Towing speed, *v* (m/s)	Door spread, *D* (m)
0.6, 0.75, 0.9	2.4, 2.8, 3.2, 3.6

The conversion process between the model net based on modified Tauti's law and the full-scale net is as follows:

$$\lambda = \frac{L_F}{L_M} \tag{14}$$

$$\lambda' = \frac{l_F}{l_M} = \frac{d_F}{d_M} \tag{15}$$

$$\frac{v_F}{v_M} = \left(\lambda'^{n+1} \times \frac{\rho_{sF} - \rho_F}{\rho_{sM} - \rho_M} \times \frac{\rho_M}{\rho_F}\right)^{\frac{1}{2-n}} \tag{16}$$

$$\frac{F_F}{F_M} = \lambda^2 \lambda' \frac{\rho_{sF} - \rho_F}{\rho_{sM} - \rho_M} \tag{17}$$

where $L, l, d, v, \rho_s, \rho,$ and F are the total stretched length, mesh size, twine diameter, speed, material density, water density, and force between the full-scale and model trawl nets. Here, n was assumed to be 0.15 for the middle trawl net [25].

Changes in the morphology of the model net were captured using cameras installed at the front end of the net mouth and the tank sidewall. These two cameras captured images of the net mouth and the side-view morphology of the net. The results are shown in Figures 5 and 6.

Fig. 5 Side view morphology of the net in the towing tank

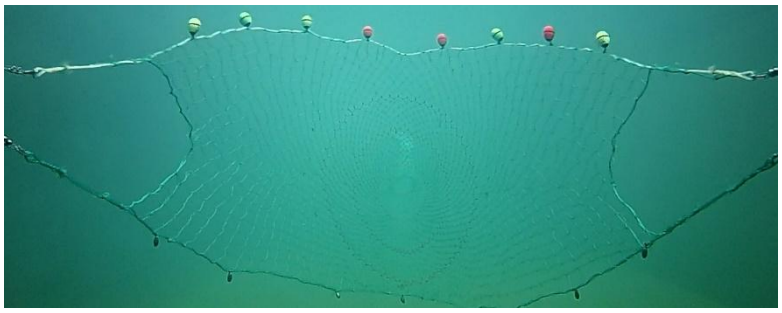

Fig. 6 Net mouth in the towing tank

For each condition, the tensile sensor measured the drag force, and after filtering through the Fourier transform, the average value of the drag force in the latter part of the trawl process was obtained. Simultaneously, the image of the stable net type was intercepted in the later period of the trawling process, and specific trawl parameters were obtained by correcting the images from which the spatial data of the net morphology were plotted. Image rectification was performed using DeFishr software [26], followed by spatial coordinate extraction of trawl feature points via a GetData Graph Digitizer [27], with equipment positioning parameters and characteristic lengths serving as scaling references.

2.4 Sea trials

The sea trials using ZHEYUKE No. 2 with a 48.8 m length, 8 m beam, 3.4 m draft, and 700 t displacement. The sea trial used oval-cambered double-slotted otter boards, each measuring 1.70 m in length, 1.43 m in width and 2.1 m^2 in area, with the otter pendant length of 2.5 m. The sea area is located in the Zhoushan Archipelago waters of China, specifically in a maritime zone near 124°E longitude and 30°N latitude, with the following environmental conditions: water depth, 70 m; wind force, Beaufort scale 6, Wave height: 1.2 m, Current velocity: 1 kn.

As shown in Figures 7 and 8, a MARPORT system sensor was employed to monitor the trawl net mouth, whereas an MFX sensor (TE/TS) was used to measure the incoming flow velocity of the trawl net. In addition, grid sensors (SS-08/09-00) were used to measure the wing end spread, and DS sensors (SS-15/16-00) were used to measure the otter board spacing (door spread). All sensor data were collected in real time.

This experiment focused on quantifying the hydrodynamic deformation characteristics of trawl nets under controlled towing speed (2-4 kn) and warp length (80-170 m) adjustments.

Fig. 7 Otter board space monitor

Fig. 8 Flow velocity and wing-end spread monitor

2.5 Data analysis

Hydrodynamic datasets derived from numerical simulations, including drag forces, energy efficiency coefficients, net mouth vertical opening, wing-end spread, and bridle angles, were analysed. Comparative assessments were conducted on trawl mouth performance metrics across varying door-spread configurations and flow velocities.

Considering the methodological disparities between numerical simulations, towing tank tests, and sea trials, this study employed generalised additive modelling (GAM) to extrapolate three key hydrodynamic parameters (net mouth vertical opening, wing end spread and drag force) from the simulation data.

A GAM [28] is a generalised linear model that allows for an extended form of the linear predictor:

$$\eta = \beta_0 + f_1(x_1) + f_2(x_2) + \cdots + + f_p(x_p) \tag{18}$$

where η is the linear predictor, β_0 is the intercept, $f_i(x_i)$ is the smooth function.

The GAM was implemented using Matlab 's Fitrgam function, with cubic spline smooth terms fitted for flow velocity and door spread as predictors. The model training utilized 5-fold cross-validation to automatically optimise the smoothing parameters of the training data. The predictive outcomes were rigorously validated against the scaled towing experimental results, with experimental data conversion performed using the modified Tauti's law, thereby verifying the fidelity of the simulation model.

During the sea trial, changes in board spacing and flow velocity occurred with variations in the flow velocity and warp length. In this study, the flow velocity, door spread, and wing-end spread at the same time points during sea trials were processed to analyse the variation in wing-end spread under different conditions.

3. Results

3.1 The result of the numerical simulations

3.1.1 Effects of flow velocity and door spread on the net mouth shape

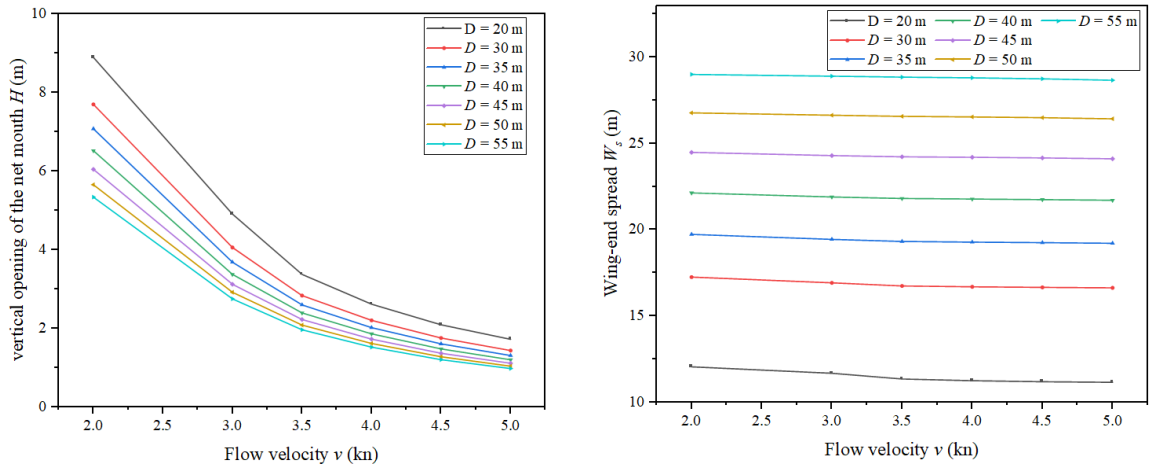

(a) Vertical opening (b) Wing-end spread

Fig. 9 Variation of the net mouth shape

As illustrated in Figure 9, the vertical opening of the net mouth decreased with an increase in the flow velocity and door spread. At a low flow velocity, the door spread significantly affected the vertical opening of the net mouth. As the flow velocity increased, the effect of door spread diminished. When the flow velocity increases from 2 kn to 5 kn, the reduction rate in the net mouth's vertical opening ($\Delta H/\Delta D$) influenced by the door spread decreases from 0.119-0.117-0.086 to 0.028-0.023-0.016, respectively, as the door spread increases from 20-30-40-50 m.

The wing-end spread increased with the expansion of the door spread and decreased with an increase in the flow velocity. The door spread plays a decisive role in determining the wing-end spread. Under the same door spread, the wing-end spread decreased gradually with increasing flow velocity, and the rate of decrease slowed down. When the flow velocity increases from 2 to 5 kn, the changes in the wing-end spread ΔW_s are 0.89, 0.62, 0.43, and 0.35 m for door spreads of 20, 30, 40, and 50 m, respectively. The average growth rate of wing-end of the net ($\Delta W_s/\Delta D$) are 0.537-0.503-0.472, with the door spread increased from 20-30-40-50 m.

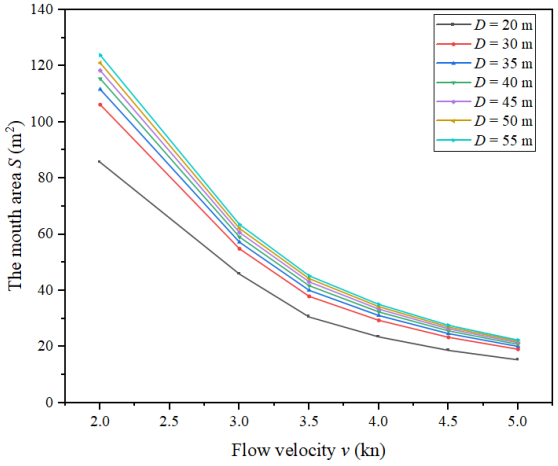

Fig. 10 Variation of the net mouth area

As shown in Figure 10, the net mouth area decreased with increasing flow velocity and increased with increasing door spread. The rate of change in the mouth area decreased with an increase in the flow velocity and door spread. When the flow velocity increases from 2 kn to 5 kn, the growth rate $(\Delta S/\Delta D)$ influenced by the door spread decreases from 2.055-0.921-0.563 to 0.373-0.176-0.107 m, respectively, as the door spread increases from 20-30-40-50 m. When the door spread is 40 m, the reduction rate decreases influenced by the flow velocity $(\Delta S/\Delta v)$ from 55.36-26.71-11.54 ms, respectively, as the flow velocity increases from 3-4-5 kn.

3.1.2 Effects of flow velocity and door spread on the drag force and energy consumption coefficient

In the numerical simulation results, the trawl drag forces under different flow velocities and door spreads were obtained directly according to Hooke's law by reading the coordinates of the endpoints of the bridle and otter boards. The results are presented in Figure 11. Based on the obtained drag-force vector $\boldsymbol{T}$, the bridge angles under different conditions were obtained using T_y/T_x, as shown in Figure 12.

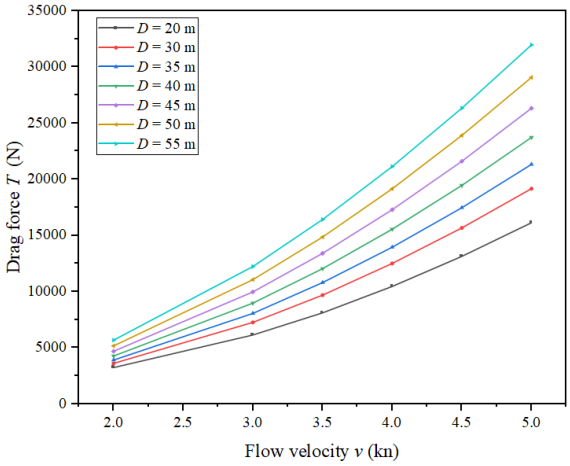

Fig. 11 Variation of the drag force of the simulation result

Under the same flow velocity conditions, the drag force of the trawl net increased with an increase in the door spread. In addition, when the door spread was constant, the drag force increased with the flow velocity. There was a positive association between the flow velocity and door spread on the trawl net drag. The drag force exhibits a nonlinear growth relationship with the flow velocity: when the flow velocity is less than 3 kN, the drag force increases slowly, and when the flow velocity is high, the drag force increases significantly faster. The increase of the door spread significantly affects the drag force, when the flow velocity is 4 kn, with the door spread increases from 20-30-40-50 m, the growth rate of drag force $(\Delta T\ /\Delta D)$ of the trawl increases from 2050-3045-3595 N/m, with the increase of the door spread, the growth rate of the drag force of the trawl also becomes larger.

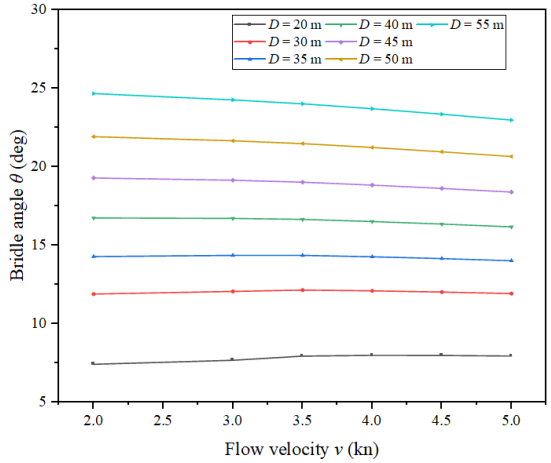

Fig. 12 Variation of the bridle angle of the simulation result

The bridle angle increases as the door spreads. At a low door spread ($D = 20$ m), the bridle angle increased with an increase in flow velocity. As the door spread increased ($D = 30, 35$ m), the bridle angle initially increased and then decreased with increasing flow velocity. At high flow velocities ($D \geq 40$ m), the bridle angle decreases as the flow velocity continues to rise. Compared with the flow velocity, the door spread plays a more dominant role in determining the bridle angle, the average bridle angle of the net are 7.81-12.01-16.52°-21.31°, with the door spread increases from 20-30-40-50 m. As the door spread increased, the influence of the flow velocity on the bridle angle became more significant. When the door spread was 55 m, the bridle angles were 24.65°, 24.25°, 23.69°, and 22.96°, at flow velocities of 2, 3, 4 and 5kn, respectively.

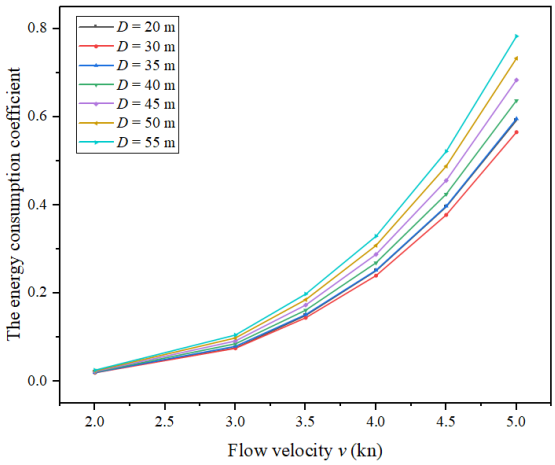

Fig. 13 Variation of the energy consumption coefficient of the simulation result

As shown in Figure 13, the energy consumption coefficient increased with increasing flow velocity. At the same flow velocity, the energy consumption coefficient initially decreased and then increased with increasing door spread. The energy consumption coefficient was minimised when the door spread was 30m. As the flow rate increased, the effect of door spread on the energy consumption coefficient increased. When the flow velocity increases from 2 kn to 5 kn, the growth rate ($\Delta C_e/\Delta D$) influenced by the door spread increases from 0.049-0.102 to 3.047-4.129 $\mathrm{m}^{-1}/1000$, respectively, as the door spread increases from 30-40-50 m.

3.2 Comparison of towing tests results and numerical simulations

Based on the modified Tauti's law, the results of the model net under different flow velocities and door spreads were converted to a full-scale trawl, as shown in Figure 14. The converted results were compared with the numerical simulation results predicted using the GAM, as shown in Figure 15.

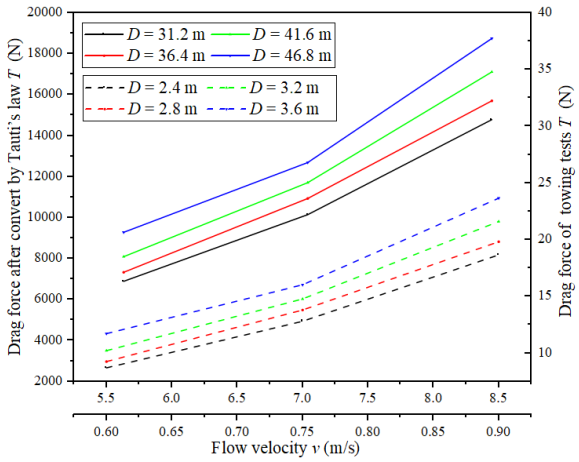

Fig. 14 The results of towing tests converted by Tauti's law

Compared to model test, the numerical simulation results are in close agreement with the test data, with a maximum error of approximately 15 %. This indicated that the numerical simulation results were reasonably reliable. At a flow velocity of 4.34 kn and door spread of 41.6 m, the difference in the wing-end spread between the numerical simulation and model test reached a maximum of 13.5 %, whereas the difference in the drag force reached 13.9 %. At a flow velocity of 4.34 kn and door spread of 46.8 m, the difference in the vertical opening of the net mouth reached a maximum of 14.8 %. The sources of error may include neglecting the interaction between the flow and trawl net during the simulation. In reality, as water flows through a trawl, it causes a corresponding velocity attenuation occurs. Additionally, vibrations of the equipment and net during high-speed towing in the model tests may have contributed to these discrepancies.

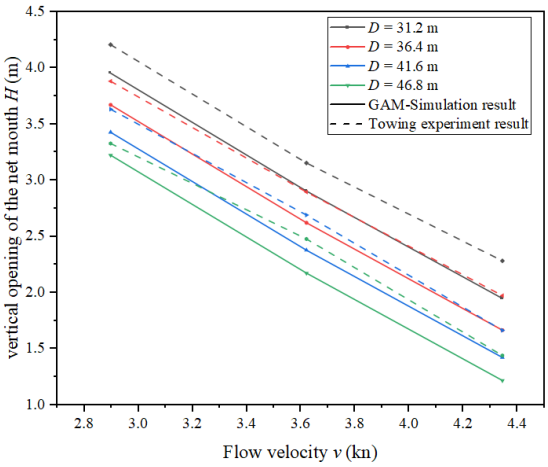

(a) vertical opening

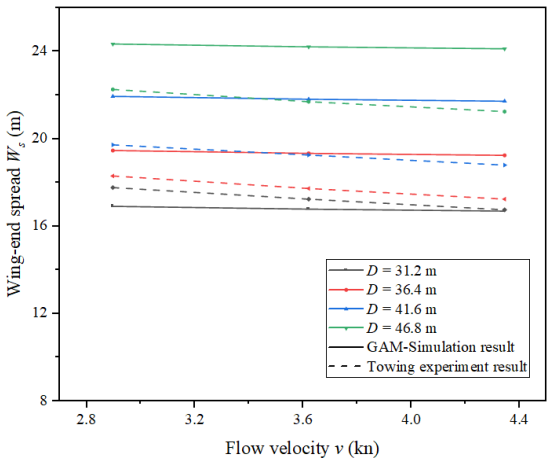

(b) Wing-end spread

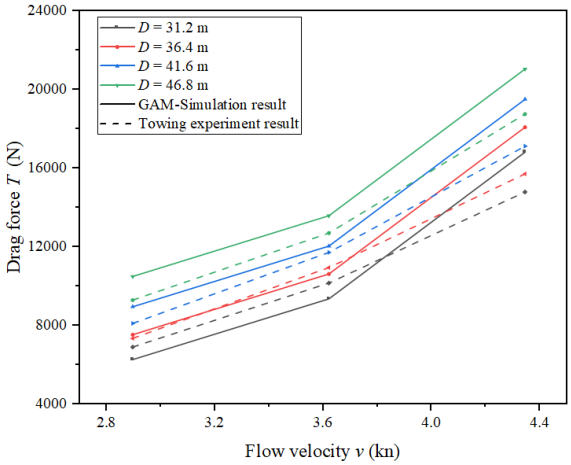

(c) Drag force

Fig. 15 Comparison between the predicted results of the simulation and the towing test

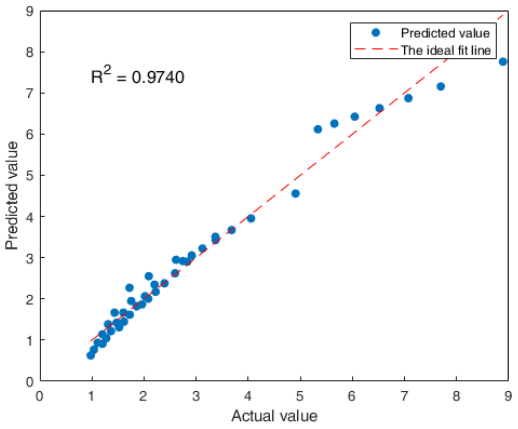

(a) vertical opening

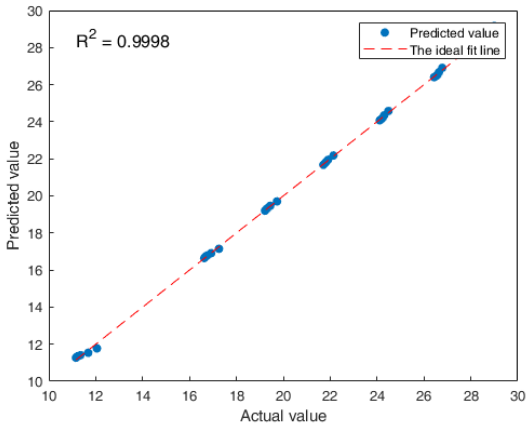

(b) Wing-end spread

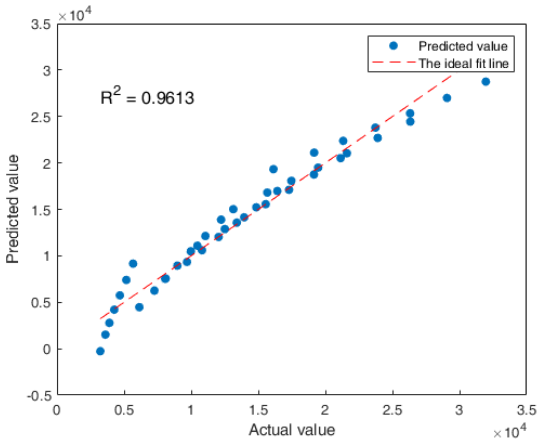

(c) Drag force

Fig. 16 Comparison of the actual and predicted values

Figure 16 presents a comparative analysis of the measured and GAM-predicted values for the test dataset. The prediction scatter plots demonstrated tightly clustered distributions with limited dispersion, reflecting the model's predictive accuracy and reliability. $R^2 = 1$ represented the perfect fit line; the R^2 values of the predicted models were higher than 0.96, indicating a robust correspondence between the simulation results and fitted curves. The scatter plots of the GAM model clearly displayed relatively stable and narrowly dispersed predicted results.

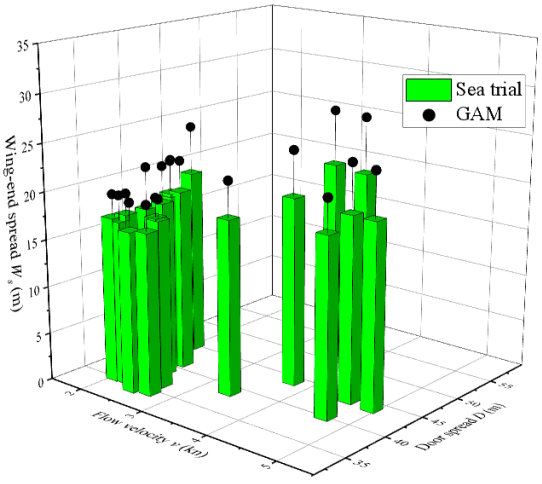

Fig. 17 Comparison of wing-end spread between the predicted and sea trial values

3.3 Comparison of sea trial results and numerical simulations

During fishing operations, the net wing-end spread is adjusted by releasing or hauling the warp and changing the towing speed. During the sea trials, the door spread ranged from 30 to 50 m, and the flow velocity ranged from to 2-5 kn.

As shown in Figure 17, the wing-end spread increased with the door spread. However, the influence of the flow velocity on the wing-end spread was relatively small. The prediction results of the GAM analyses were similar to those of the sea trial experiment. The flow velocity significantly influenced the accuracy of the prediction results; the smaller the flow velocity, the closer the prediction results were to the actual results. When the flow velocity was less than 3kn, all predicted results differed from the actual results by less than 15 %. Overall, the measured results of the sea trial were consistently smaller than the predicted results, with a difference of 20 %.

During the sea trial, the complex and variable natural environment may have led to measurement deviations, and the effect of catch on the nets was neglected during the trial.

4. Discussion

To improve trawl net fishing efficiency, maximising the net mouth opening while managing energy use during operations is crucial. This study evaluated the impact of different door spread configurations and flow velocities on the net mouth performance and trawl drag forces. The findings revealed the hydrodynamic behaviour of the net mouth when subjected to changing door spreads and flow velocities, showing patterns that aligned with the results of Thierry et al. [8].

Based on the numerical simulation results, the empirical formulas for the trawl parameters with respect to door spread and flow velocity were obtained through polynomial fitting:

$$H = 23.312 - 7.387v - 0.193D + 0.647v^2 + 0.001D^2 + 0.027vD \quad (19)$$

$$W_s = 1.688 - 0.689v + 0.594D + 0.043v^2 - 0.002D^2 + 0.006vD \quad (20)$$

$$S = 210.095 - 96.530v + 2.306D + 11.004v^2 - 0.012D^2 - 0.261vD \quad (21)$$

$$T = 12161 - 4690v - 446D + 875v^2 + 3.2D^2 + 130vD \quad (22)$$

In this study, the influence of door spread and flow velocity on the vertical opening of the net mouth exhibited a nonlinear coupling relationship, as shown in equation (20-21). At low flow velocities, the geometric effects dominate. As the door spread increases, the wing-end spread is enhanced; however, owing to the constraints imposed by the fixed structure, the vertical opening significantly decreases because of geometric limitations. At high flow velocities, the hydrodynamic effects become the key factor, and the dynamic pressure exerted by the flow on the trawl net increases, leading to a stronger inhibitory effect on the vertical expansion of the net mouth. The door spread is the core parameter determining the wing-end spread, and trawl nets with a larger door spread exhibit stronger resistance to the compressive effects of the flow velocity.

In equation (22), the flow velocity and door spread have a significant impact on the net mouth area, which is a key factor affecting the fishing performance of trawl nets. As part of the net body, the net mouth determines the initial catch volume during the early stages of trawling. In addition, the shape of the anterior net body affects the catch escape. In practical fishing operations, a larger net mouth area leads to a higher fishing efficiency.

The drag force in a trawl is contingent on the deformation and motion of the trawl net, door spread, and flow velocity. The equation (23) demonstrates that the net drag force exhibits a nonlinear growth pattern in response to the increasing flow velocity and expanded door spread. The coefficient of energy consumption plays a pivotal role in the design of a trawl net, as it has the potential to markedly diminish resistance, which in turn can lead to a reduction in fuel usage and an enhancement of fishing efficiency [29]. Using a low towing

speed and door spread can achieve a smaller drag force; however, as the door spread decreases, the net mouth area decreases, thereby reducing fishing efficiency. An optimal range of door spreads exists that can maximise the performance and minimise the energy consumption at specific flow velocities.

In contrast to numerical simulations, the towing test process involves intricate interactions between the trawl net, water flow, and tension. Studies utilising ECVM to monitor flow velocities across different sections of a trawl net in a flume tank revealed a 23 % difference in flow velocity between the wings and the body net, and a 5 % difference compared to the central region of the net body [6]. Furthermore, influenced by hydrodynamic forces, the trawl net exhibits oscillatory behaviour that is amplified with increasing door spread. The interaction between the incoming flow and the trawl net was significantly modulated by the door spread. The use of the fluid-structure interaction method [30] can effectively analyse the interaction relationship between the trawl and flow and improve the computational accuracy of the simulation. Compared with towing tank tests and numerical simulations, sea trials conducted in actual marine environments provide the most authentic fishing performance data. However, sea trial experiments are subject to uncertainty owing to the variability in oceanic conditions, equipment limitations, and operational uncontrollability [31, 32].

During actual trawling operations, otter boards spread through the combined effects of warp and towing speeds. The door spread can be modulated by adjusting the warp length and towing speed; both reducing the towing speed and increasing the warp length effectively enhance the door spread [33]. Notably, net fishing performance demonstrates a dual dependence on door spread and flow velocity. Furthermore, the hydrodynamic characteristics of the otter boards exhibited significant configuration dependencies. Future studies could further explore the integration of computational fluid dynamics (CFD) with the lumped mass method to refine the hydrodynamic models of trawl systems. This includes enhancing the analysis of otter board hydrodynamics under dynamic conditions and quantifying the coupled effects of trawl tension and net plate movement on trawler stability and energy efficiency. The coupled computational fluid dynamics and lumped mass method enable holistic trawl system analysis by simultaneously resolving otter board hydrodynamics and quantifying trawl tension effects on trawler performance [34] during fishing operations.

5. Conclusion

The lumped-mass method was applied to numerically model midwater trawl nets, with a particular focus on how door spread, and flow velocity affect trawl performance. This study examined the trawl geometry parameters, including the vertical opening of the net mouth, wing-end spread, and mouth area, under various operational conditions. Performance metrics such as the trawl drag force, energy consumption coefficient, and bridle angle were also analysed. The main findings are as follows.

(1) The vertical opening of the net mouth exhibited an inverse relationship with the flow velocity and door spread. The wing-end spread expanded proportionally to the door spread but contracted at higher flow velocities.

(2) Larger door spreads enhanced the net mouth area, whereas higher flow velocities reduced it.

(3) Both elevated doors spread, and flow velocity contributed to higher trawl net drag force.

(4) The energy consumption coefficient increased with the flow velocity. For fixed velocities, the energy consumption coefficient initially decreased and then increased as the door spread increased.

This study investigates trawl nets using numerical simulations, model tests, and sea trials. The results demonstrate that the accuracy of net configuration calculations depends on multiple factors. The rapid iteration capability of numerical simulations, intuitiveness of model tests, and comprehensiveness of sea trials collectively establish the integrated use of these three methods as an optimal approach for trawl system development.

Based on numerical simulations, generalised additive models were employed to predict trawl performance. These predictions are validated through a comparative analysis of towing tank tests and sea trials, confirming the reliability of the simulation results. This method effectively and efficiently predicts the net configuration under unknown working conditions and provides valuable guidance for optimal fishing net deployment strategies.

ACKNOWLEDGMENTS

This study was financially supported by the “Pioneer” and “Leading Goose” R&D Program of Zhejiang (2022C03023).

REFERENCES

[1] FAO, 2022. The state of world fisheries and aquaculture 2022. Towards blue transformation. *Food and Agriculture Organization of the United Nations*, Rome, Italy.

[2] Standing Committee of the National People's Congress, 2023. Fisheries Law of the People's Republic of China (2023 Revision). *China Legal Publishing House*, Beijing, China.

[3] Sun, X., Yin, Y., Jin, Y., Zhang, X., Zhang, X., 2011. The modeling of single-boat, mid-water trawl systems for fishing simulation. *Fisheries Research*, 109(1), 7-15. https://doi.org/10.1016/j.fishres.2010.12.027

[4] Yao, Y., Chen, Y., Zhou, H., Yang, H., 2016. A method for improving the simulation efficiency of trawl based on simulation stability criterion. *Ocean Engineering*, 117, 63-77. https://doi.org/10.1016/j.oceaneng.2016.03.031

[5] Nguyen, T. X., Winger, P. D., Orr, D., Legge, G., Delouche, H., Gardner, A., 2015. Computer simulation and flume tank testing of scale engineering models: How well do these techniques predict full scale at-sea performance of bottom trawls? *Fisheries Research*, 161, 217-225. https://doi.org/10.1016/j.fishres.2014.08.007

[6] Tang, H., Thierry, N. N. B., Achille, N. P., Mouangue, R., Xu, L., Hu, F., Mbangue, E., 2024. Coupled dynamics of the moving Antarctic krill trawl structure and its hydrodynamics behavior using various catch sizes and door spreads based on wavelet-based and Fourier analysis. *Journal of Fluids and Structures*, 124, 104037. https://doi.org/10.1016/j.jfluidstructs.2023.104037

[7] Thierry, N. N. B., Tang, H., Liuxiong, X., You, X., Hu, F., Achile, N. P., Kindong, R., 2020. Hydrodynamic performance of bottom trawls with different materials, mesh sizes, and twine thicknesses. *Fisheries Research*, 221, 105403. https://doi.org/10.1016/j.fishres.2019.105403

[8] Thierry, N. N. B., Tang, H., Pandong, A. N., Xu, L., Adekunle, D. M., Hu, F., 2022. Examining engineering performance of midwater trawl with different horizontal spread ratio, floatage, and weight parameters: A case study of model net for Antarctic krill fisheries. *International Journal of Naval Architecture and Ocean Engineering*, 14, 100448. https://doi.org/10.1016/j.ijnaoe.2022.100448

[9] Sala, A., Carlo, D., Buglioni, G., Lucchetti, A., 2011. Energy performance evaluation of fishing vessels by fuel mass flow measuring system. *Ocean Engineering*, 38(7), 804-809. https://doi.org/10.1016/j.oceaneng.2011.02.004

[10] Jia, P., Xu, H., Du, Z., Xie, Y., Zhao, C., 2024. Prediction of net mouth area for trawlers based on sea trials and machine learning. *Ocean Engineering*, 293, 116266. https://doi.org/10.1016/j.oceaneng.2023.116266

[11] Priour, D., 1999. Calculation of net shapes by the finite element method with triangular elements. *Communications in Numerical Methods in Engineering*, 15, 755-763. https://doi.org/10.1002/(SICI)1099-0887(199910)15:10<755::AID-CNM299>3.0.CO;2-M

[12] Zhao, Y., Bi, C., Dong, G., Gui, F., Cui, Y., Guan, C., Xu, T., 2013. Numerical simulation of the flow around fishing plane nets using the porous media model. *Ocean Engineering*, 62, 25-37. https://doi.org/10.1016/j.oceaneng.2013.01.009

[13] Ye, X., Chen, X., Chen, S., Wang, T., 2014. Research on the visual dynamic simulation technology of fishing net. *2014 IEEE International Conference on Mechatronics and Automation*, Tianjin, China, 1929-1934. https://doi.org/10.1109/ICMA.2014.6885997

[14] Thierry, N. N. B., Tang, H., Xu, L., Hu, F., Dong, S., Achille, N. P., Zou, B., 2021. Comparison between physical model testing and numerical simulation using two-way fluid-structure interaction approach of new trawl design for coastal bottom trawl net. *Ocean Engineering*, 233, 109112. https://doi.org/10.1016/j.oceaneng.2021.109112

[15] Kim, Y. H., 2012. Analysis of turbulence and tilt by in-situ measurements inside the codend of a shrimp beam trawl. *Ocean Engineering*, 53, 6-15. https://doi.org/10.1016/j.oceaneng.2012.06.014

[16] Kim, Y. H., 2013. Analysis of the turbulent flow and tilt in the codend of a bottom trawl during fishing operations. *Ocean Engineering*, 64, 100-108. https://doi.org/10.1016/j.oceaneng.2013.02.019

[17] Priour, D., Prada, D. L. A., 2015. An experimental/numerical study of the catch weight influence on trawl behavior. *Ocean Engineering*, 94, 94-102. https://doi.org/10.1016/j.oceaneng.2014.11.016

[18] Wan, R., Guan, Q., Huang, L., Li, Z., Zhou, C., Wang, L., Jia, M., 2021. Effects of otter board and cable length on hydrodynamic performance of Antarctic krill trawl system. *Ocean Engineering*, 236, 109408. https://doi.org/10.1016/j.oceaneng.2021.109408

[19] Park, H. H., 2007. A method for estimating the gear shape of a mid-water trawl. *Ocean Engineering*, 34(3-4), 470-478. https://doi.org/10.1016/j.oceaneng.2006.03.001

[20] You, X., Hu, F., Zhuang, X., Dong, S., Shiode, D., 2021. Effect of wingtip flow on hydrodynamic characteristics of cambered otter board. *Ocean Engineering*, 222, 108611. https://doi.org/10.1016/j.oceaneng.2021.108611

[21] Takagi, T., Shimizu, T., Suzuki, K., Hiraishi, T., Yamamoto, K., 2004. Validity and layout of NaLA a net configuration and loading analysis system. *Fisheries Research*, 66 (23), 235–243. https://doi.org/10.1016/S0165-7836(03)00204-2

[22] Kemal, B., Deniz, B.B., 2024. Investigation into forces on offshore piles with constant and linearly varying diameters using CFD and extended Morison equation under separate wave and current loadings, *Brodogradnja*, 75(4), 75406. https://doi.org/10.21278/brod75406

[23] Zhou, C., Xu, L.X., Zhang, X.F., Ye, X.C., 2014. Application of numerical simulation for analysis of sinking characteristics of purse seine. *Journal of Ocean University of China*, 14 (1), 135–142. https://doi.org/10.1007/s11802-015-2384-8

[24] Xu, L., 2004. Theory and design of fishing gear. *China Agriculture Press*, Beijing, China.

[25] Hu, F., Matuda, K., Tokai, T., 2001. Effects of drag coefficient of netting for dynamic similarity on model testing of trawl nets. *Fisheries Science*, 67(1), 84-89. https://doi.org/10.1046/j.1444-2906.2001.00203.x

[26] ProDAD, GmbH. Defishr V1. Software available at http://www.prodad.de/register.html

[27] GetData Graph Digitizer version 2.25.0.32. Software available at https://getdata-graph-digitizer.com

[28] Venables, W.N., Dichmont, C.M., 2004. GLMs, GAMs and GLMMs: an overview of theory for applications in fisheries research, *Fisheries Research*, 70(2–3), 319-337. https://doi.org/10.1016/j.fishres.2004.08.011

[29] Balash, C., Sterling, D., 2012. Prawn trawl drag due to material properties an investigation of the potential for drag reduction. *Proceedings of the 2nd International Symposium on Fishing Vessel Energy Efficiency E-Fishing*, Vigo, Spain, 22-24 May, 9.

[30] Jiao, J., Chen, Z., Xu, S., 2024. CFD-FEM simulation of water entry of aluminium flat stiffened plate structure considering the effects of hydroelasticity. *Brodogradnja*, 75(1), 75108. https://doi.org/10.21278/brod75108

[31] Fiorentini, L., Sala, A., Hansen, K., Cosimi, G., Palumbo, V., 2004. Comparison between model testing and full-scale trials of new trawl design for Italian bottom fisheries. *Fisheries Science*, 70(2), 349-359. https://doi.org/10.1111/j.1444-2906.2004.00813.x

[32] Sala, A., Lucchetti, A., Palumbo, V., Hansen, K., 2008. Energy saving trawl in Mediterranean demersal fisheries. *Maritime Industry, Ocean Engineering and Coastal Resources. Taylor & Francis Group*, London, UK, 961-964.

[33] Zhao, Y., Mao, Y., Liu, B., Liu, C., 2016. Three-dimensional tracking control of mid-water trawl system based on backstepping method. *3rd International Conference on Information Science and Control Engineering*, Beijing, China, 1164-1168. https://doi.org/10.1109/ICISCE.2016.250

[34] Zhao, C., Wang, W., Jia, P., Xie, Y., 2021. Optimisation of hull form of ocean-going trawler. *Brodogradnja*, 72(4), 33-46. https://doi.org/10.21278/brod72403